

Revision 1

Word count: 8464

Effect of cationic substitution on the pressure-induced phase transitions in calcium carbonate

Naira S. Martirosyan^{1,2}, Ilias Efthimiopoulos¹, Lea Pennacchioni^{1,3}, Richard Wirth¹,
Sandro Jahn², Monika Koch-Müller¹

¹ GFZ German Research Centre for Geosciences, Telegrafenberg, 14473 Potsdam, Germany

² Institute of Geology and Mineralogy, University of Cologne, Zùlpicher Str. 49b, 50674 Cologne, Germany

³ Institute of Geosciences, Goethe University, Altenhöferallee 1, 60438 Frankfurt am Main, Germany

*Corresponding author: naira.martirosyan@gfz-potsdam.de

Abstract

The high-pressure CaCO₃ phase diagram has been the most extensively studied within the carbonates group. However, both the diverse mineralogy of carbonates and the abundance of solid solutions in natural samples require the investigation of multi-component systems at high pressures (*P*) and temperatures (*T*). Here we studied a member of the CaCO₃ – SrCO₃ solid solution series, and revealed the effect of substituting Ca²⁺ with Sr²⁺ on the pressure-induced phase transitions in calcium carbonate.

A synthetic solid solution $\text{Ca}_{0.82}\text{Sr}_{0.18}\text{CO}_3$ was studied in situ by Raman spectroscopy in a diamond anvil cell (DAC) up to 55 GPa and 800 K. The results of this work show significant differences in the high-pressure structural and vibrational behavior of the (Ca, Sr) CO_3 solid solution compared to that of pure CaCO_3 . The monoclinic CaCO_3 -II – type structure (Sr-calcite-II) was observed already at ambient conditions instead of the ‘expected’ rhombohedral calcite. The stress-induced phase transition to a new high-pressure modification, termed here as Sr-calcite-IIIc, was detected at 7 GPa. Sr-calcite-VII formed already at 16 GPa and room T , which is 14 GPa lower compared to CaCO_3 -VII. Finally, crystallization of Sr-aragonite was detected at 540 K and 9 GPa, at 200 K lower T than pure aragonite. Our results indicate that substitution of Ca^{2+} by bigger cations, such as Sr^{2+} , in CaCO_3 structures can stabilize phases with larger cation coordination sites (e.g. aragonite, CaCO_3 -VII, and post-aragonite) at lower $P - T$ conditions compared to pure CaCO_3 . The present study shows that the role of cationic composition in the phase behavior of carbonates at high pressures should be carefully considered when modeling the deep carbon cycle and mantle processes involving carbonates, such as metasomatism, deep mantle melting, and diamond formation.

Key words: deep carbon cycle, calcium carbonate, solid solution, phase diagram, phase transition, high pressure, vibrational spectroscopy

Introduction

Investigations of natural samples, mantle xenoliths, carbonatites, and kimberlites, inclusions in diamonds and carbonate-bearing rocks from the ultrahigh-pressure metamorphic terranes, provide direct evidence of the existence of carbonates and carbonatite melts in the

Earth's deep upper mantle, transition zone, and lower mantle (Stachel et al., 2000; Brenker et al., 2007; Logvinova et al., 2008, 2011, 2019a, b; Kaminsky et al., 2009, 2013; Korsakov et al., 2009; Kamenetsky and Yaxley, 2015; Sharygin et al., 2015). Syngenetic inclusions in diamonds and other mantle minerals contain frequently calcium carbonates, dolomite, magnesite, and ankerite (Stachel et al., 2000; Brenker et al., 2007; Logvinova et al., 2008, 2011, 2019a, b; Kaminsky et al., 2009, 2013; Korsakov et al., 2010). The abundance of the calcium carbonate at near surface and mantle conditions, and its overall geological significance has triggered an enormous interest in the CaCO_3 phase diagram (Suito et al., 2001; Ono et al., 2005, 2007; Merlini et al., 2012, 2018; Pippinger et al., 2014; Koch-Müller et al., 2016; Gavryushkin et al., 2017; Lobanov et al., 2017; Bayarjargal et al., 2018; etc.).

At atmospheric pressure CaCO_3 crystallizes predominantly in the rhombohedral calcite structure (space group (SG) $R\bar{3}c$) with coplanar CO_3^{2-} groups and Ca^{2+} in 6 – fold coordination ($\text{Ca}^{[6]}$). Compression of calcite leads to a complex polymorphism with several phase transitions. Previous experimental and computational studies revealed four stable high-pressure polymorphs of calcite: aragonite (SG $Pnma$, $\text{Ca}^{[9]}$), CaCO_3 -VII (SG $P2_1/c$, $\text{Ca}^{[10]}$), post-aragonite (SG $Pmmn$, $\text{Ca}^{[12]}$), and sp^3 - CaCO_3 (SG $P2_1/c$, $\text{Ca}^{[12]}$, $\text{C}^{[4]}$) (Fig. 1) (Ono et al., 2005, 2007; Gavryushkin et al., 2017; Lobanov et al., 2017; Bayarjargal et al., 2018). The formation of these high-pressure phases is kinetically hindered at ambient temperature and occurs only above 773 K (500 °C) (Bayarjargal et al., 2018).

Cold compression of calcite, on the contrary, leads to a different sequence of high-pressure polymorphs: CaCO_3 -II (SG $P2_1/c$, $\text{Ca}^{[6]}$); CaCO_3 – III and IIIb (SG $P\bar{1}$, $\text{Ca}^{[7]}$ and $\text{Ca}^{[9]}$); CaCO_3 -VI (SG $P\bar{1}$, $\text{Ca}^{[7+2]}$) (Fig. 1) (Suito et al., 2001; Merlini et al., 2012, 2018; Koch-Müller et al., 2016; Bayarjargal et al., 2018). All of these high-pressure modifications are considered

metastable (Suito et al., 2001; Merlini et al., 2012, 2018; Koch-Müller et al., 2016; Bayarjargal et al., 2018). Such consideration arises from the fact that those polymorphs appear within the stability fields of aragonite and CaCO₃-VII, yet density-functional theory (DFT) calculations predict that they have higher enthalpies at 0 K and lower densities than aragonite and CaCO₃-VII (Koch-Müller et al., 2016; Gavryushkin et al., 2017; Bayarjargal et al., 2018).

The CaCO₃ system is well studied both at near surface conditions and at high pressures (Fig. 1). However, the mineralogy of carbonates is more diverse, and natural calcium carbonates are often found as solid solutions with Mg²⁺, Fe²⁺, Sr²⁺, Ba²⁺, Na⁺, and K⁺. The calcium carbonate solid solutions are widely used in geochemistry. For instance, Sr²⁺ incorporation into CaCO₃ is of particular interest for paleoceanographic reconstructions, isotope chemostratigraphy, and constrains of the absolute age of the sedimentary sequences with poor biostratigraphic control (Kuznetsov et al., 2014).

The diversity of carbonate compositions found in diamond inclusions and in other mantle minerals reflects the rich mantle mineralogy of carbonates. Besides (Ca, Mg, Fe)-carbonates, they may contain nyerereite (Na₂Ca(CO₃)₂) (Kaminsky et al., 2009), bütschliite (K₂Ca(CO₃)₂) (Logvinova et al., 2019b) and other sodium- and potassium-bearing carbonates, as well as a variety of (Ba, Ca)CO₃, (Sr, Ca)CO₃ and (Ca, Ba, Sr)CO₃ (Logvinova et al., 2008, 2011, 2019a; Kaminsky et al., 2009). Concentrations of Ba²⁺ and Sr²⁺ in natural calcium carbonate inclusions in diamonds and other mantle minerals can vary from a few hundredths of mole percent (0.06–0.7 mol%) (Kaminsky et al., 2009; Korsakov et al., 2010) to highly enriched varieties (5–18 mol%) (Klein-BenDavid, 2006, 2009; Logvinova et al., 2008, 2011, 2019a). It has been proposed that the high concentration of Ba²⁺ and Sr²⁺ could be a strong indication of deep metasomatic processes (Logvinova et al., 2008, 2011, 2019a).

Given the significant role of carbonates in mantle processes, such as partial melting of peridotites and eclogites (Dasgupta and Hirschmann, 2006; Kiseeva et al., 2013), metasomatism (Yaxley et al., 1991; Kiseeva 2012) and diamond formation (Palyanov et al., 1999; Stachel and Harris, 2008), and the diversity of compositions found in natural samples, studies of phase diagrams at different $P - T$ conditions in the multicomponent carbonate systems are of great importance.

The solid solution systems $\text{CaCO}_3 - \text{SrCO}_3$ and $\text{CaCO}_3 - \text{BaCO}_3$ are poorly studied at high pressures. Unlike CaCO_3 , the end members SrCO_3 and BaCO_3 have simple phase diagrams. They crystallize in the orthorhombic aragonite structure up to 22 GPa (SrCO_3) and 10 GPa (BaCO_3), and transform to post-aragonite with further pressure increase (Wang et al., 2015). The binary $\text{CaCO}_3 - \text{SrCO}_3$ system has been studied at $P - T$ conditions up to 1.6 GPa and 923 K (650 °C) (Carlson, 1980). It was demonstrated that small amounts of Sr^{2+} expand the stability region of the aragonite phase.

In order to better understand the role played by the Sr^{2+} substitution on the complex polymorphism of calcium carbonate at mantle pressures and temperatures, more experimental work has to be performed on the CaCO_3 - SrCO_3 system at extreme conditions. In this study we synthesized a $(\text{Ca}, \text{Sr})\text{CO}_3$ solid solution at 2 GPa and 1273 K and conducted in situ high-pressure and temperature experiments up to 55 GPa and 800 K in diamond anvil cells using Raman spectroscopy.

Experimental methods

Sample synthesis and characterization

(Ca, Sr)CO₃ solid solution was synthesized at 2 GPa and 1273 K (1000 °C) (Fig. 1) in a Walker type multi-anvil apparatus at GFZ Potsdam (Walker et al., 1990). The run duration was 8 h. The starting material was prepared from analytical grade synthetic powders of CaCO₃ and SrCO₃ (99.999% purity, Sigma Aldrich Chemical Company), with the concentration of SrCO₃ 20 mol% in the initial mixture. The blended mixture was placed into a Pt capsule. A Cr-doped MgO octahedron with an edge length of 18 mm and other MgO-based parts were used as pressure transmitting media. Heat was generated with a stepped graphite heater. Temperature was controlled using a W_{5%}Re-W_{26%}Re type C thermocouple. Eight tungsten carbide cubes with the truncation edge length of 11 mm were used as Kawai-type anvils. The sample was analyzed by electron microprobe (EMP), transmission electron microscopy (TEM), powder X-ray diffraction (XRD), Fourier-transform infrared (FTIR), and Raman spectroscopy.

The chemical composition of the synthesized sample (Supplementary materials Table S1; Fig. S2) was determined with EMP analyses using a JEOL Hyperprobe JXA-8500F EMP with a field emission cathode (GFZ, Potsdam). Analysis was conducted at a 15 kV acceleration voltage, a 10nA beam current, and a 0.5-10 μm beam size. Dolomite and strontianite were used as standards.

TEM with a high-resolution energy-dispersive spectrometer was used for the microtexture observation and preliminary structural analysis (Fig. 2; S3). Thin sections of approximately 15×10×0.15 μm³ size were prepared with a focused Ga-ion beam (FIB) system (FEI FIB 200 TEM) (Wirth, 2009) directly from the crystals in the microprobe mounts, and analyzed in a FEI Tecnai G2 F20 X-Twin transmission electron microscope (GFZ, Potsdam).

The structural analysis was performed with XRD. The XRD patterns were measured at atmospheric pressure using a STOE Stadi P diffractometer equipped with a curved Germanium

(111) primary monochromator, a high resolution MYTHEN-detector and a normal focus Cu X-ray tube (Cu-K α_1 radiation) (GFZ, Potsdam). The XRD data were processed with the GSAS software package (Larson and Von Dreele 1987). Unit-cell parameters were obtained by Le Bail/Pawley refinements (Fig. 3).

FTIR measurements in the mid-infrared region were conducted with the Vertex 80v FTIR spectrometer combined with a Hyperion 2000 microscope (GFZ, Potsdam) within a 500–2000 cm $^{-1}$ spectral range (Fig. 4; S4). We used a KBr beamsplitter and a mercury–cadmium–telluride detector. The spectra were averaged over 1536 scans with a spectral resolution of 2 cm $^{-1}$. The description of the Raman measurements is given in the section below.

High pressure in situ experiments

Pressure-induced phase transitions in the Ca $_{0.82}$ Sr $_{0.18}$ CO $_3$ solid solution were studied *in situ* using Raman spectroscopy at room and at high temperatures up to 800 K (Fig. 1; S1). Two different types of diamond anvil cells (DACs) were employed, depending on the target temperature.

Symmetric piston cylinder DACs with 250 μ m culet size diamonds were used for the room temperature experiments. Rhenium gaskets were indented to a thickness of 30 – 40 μ m, and drilled in the center of the indentation to form a sample chamber. The crystals were carefully selected, cleaned with ethanol, and placed into the sample chamber together with ruby spheres acting as pressure sensors. Liquid argon (Ar) was loaded cryogenically as a pressure-transmitting medium, following the same procedure as in Koch-Müller et al. (2016). Pressure was measured using laser-induced fluorescence spectroscopy of ruby (Al $_2$ O $_3$:Cr $^{3+}$) (Dewaele et al., 2008). Previous studies have shown that the ruby scale is accurate within 2-5 % up to 55 GPa (Dewaele

et al., 2008). Four different experimental high-pressure runs were conducted at room temperature (Fig. 1; S1). Raman spectra were measured in 1 – 2 GPa steps up to 55 GPa, both on compression and decompression cycles (Fig. S1).

The second set of experiments was performed using an internally heated membrane-driven DAC (DAC – HT) (Diacell μ ScopeDAC HT (G), EasyLab, UK), equipped with diamonds of 300 μ m culet size. The measurements were carried out in the 9–10 GPa pressure range and at high temperatures from 540 K to 800 K (Fig. 1). The sample, together with $\text{SrB}_4\text{O}_7\text{:Sm}^{2+}$ powder and ruby spheres used as $P - T$ sensors, was sandwiched between two NaCl layers and placed inside the sample chamber. NaCl served both as a pressure medium and as a thermal insulator. The temperature in the DAC – HT experiments was measured both outside the sample chamber with a K – type thermocouple placed close to the lower diamond, as well as inside the sample chamber using the fluorescence lines of $\text{SrB}_4\text{O}_7\text{:Sm}^{2+}$ and ruby (Datchi et al., 2007). Details of the temperature calibrations are given in Supplementary materials. The P - T calibration method allows to determine pressure with a 0.4 - 1.2% and temperature with a 1.0-1.3% accuracy up to 20 GPa and 900 K (Datchi et al., 2007; Romanenko et al., 2018). The temperature outside the gasket hole, measured by the thermocouple, was always lower than that estimated inside the sample chamber, with the difference reaching about 50 K at the maximum temperature of 800 K.

The Raman spectra in both room and high T experiments were measured with a HORIBA Jobin Yvon LabRAM HR800 VIS spectrometer (GFZ, Potsdam) equipped with a blue 473 nm diode-pumped solid-state laser. The spectral range for the measurements was 140–1200 cm^{-1} and the data acquisition time was 120 s. The spectra were collected at ambient conditions before and after the pressure increase and at high pressures both upon compression and decompression (Fig.

S1). The measurements at high temperature were performed every 2-5 min. The software Fityk (Wojdyr, 2010) was used for data analysis.

Experimental results

Characterization of the synthesized (Ca, Sr)CO₃ solid solution

Backscattered electron images of the synthesized samples are presented in Fig. S2. The recovered sample consists of large ($\geq 30 - 100 \mu\text{m}$) grains of (Ca, Sr)CO₃ solid solution with homogeneous composition and Sr²⁺ content of 18 mol% according to the EMP analyses (Table S1). Some of the grains contain small inclusions, $\leq 1 - 2 \mu\text{m}$ in size, located primarily in voids and cracks (Fig. S2b).

Two thin films from different grains were prepared for the TEM analysis by the focused ion beam method (Fig. 2; S3). The samples have a high density of dislocations and a lamellar texture with clear interfaces caused by complex twinning (Fig. 2a). Analytical TEM confirmed that both samples have homogeneous compositions and consist predominantly of crystalline Ca-rich (Ca~80 mol%) (Ca, Sr)CO₃ solid solution (Fig. S3a, c). The electron diffraction pattern of the main phase was refined in the rhombohedral calcite unit cell; however, we see several additional low intensity reflections (Fig. 2b). The few grains of the secondary Sr-rich (Sr, Ca)CO₃ phase, that constitutes less than 1 vol% of the thin film, were detected as small inclusions along the dislocations and cracks (Fig. S3a, b). The electron diffraction pattern of the secondary phase could be refined with orthorhombic symmetry.

Most of the reflections in the XRD pattern of the Ca_{0.82}Sr_{0.18}CO₃ solid solution, including the most intense one, can be refined in the calcite structure (Fig. 3a, b) with lattice parameters $a = 5.01 \text{ \AA}$, $c = 17.25 \text{ \AA}$ (residual factor $wR_p=19\%$). However, several low intensity peaks located at

204 $2\theta = 23^\circ, 36^\circ, 47^\circ$, and 48° show a splitting incompatible with the calcite structure (Fig. 3a, b).
205 The attempts to include an orthorhombic phase, as observed in the TEM analyses, did not
206 improve the XRD refinement. It is likely that due to the low concentration, the secondary phase
207 does not appear in the XRD pattern. The best fit for all of the observed Bragg peaks was achieved
208 using a monoclinic unit cell similar to that of $\text{CaCO}_3\text{-II}$ ($wR_p=8.3\%$, Fig. 3c, d) (Merrill and
209 Bassett, 1975). The refined unit cell of $\text{Ca}_{0.82}\text{Sr}_{0.18}\text{CO}_3$ solid solution has $P2_1/c$ space group with
210 the following lattice parameters: $a = 6.44 \text{ \AA}$; $b = 5.02 \text{ \AA}$; $c = 8.13 \text{ \AA}$; $\beta = 108.13^\circ$. For
211 comparison, the lattice parameters of pure $\text{CaCO}_3\text{-II}$ are $a = 6.33 \text{ \AA}$; $b = 4.95 \text{ \AA}$; $c = 8.03 \text{ \AA}$; $\beta =$
212 107.9° at 1.5 GPa (Merrill and Bassett, 1975).

213 The difference in the structure of the synthesized solid solution from that of calcite was
214 also indicated by the results of the mid – infrared (MIR) and Raman measurements (Fig. 4, 5; S4-
215 S6). The vibrational spectrum of calcite contains 4 fundamental internal modes, assigned to CO_3^{2-}
216 vibrations: symmetric stretching (ν_1), out-of-plane bending (ν_2), asymmetric stretching (ν_3), and
217 in-plane bending (ν_4) (White, 1974) (Fig. 4; S5). The ν_1 and ν_2 modes are Raman- (ν_1) or
218 infrared- (ν_2) active only, while the ν_3 and ν_4 bands can be detected in both Raman and IR spectra
219 (White, 1974).

220 The fundamental modes in the MIR- spectrum of pristine CaCO_3 calcite are located at 872
221 cm^{-1} (ν_2), 1407 cm^{-1} (ν_3), and 712 cm^{-1} (ν_4) (Fig. 4) (White, 1974; Vahur et al., 2016).
222 Additionally, spectra can exhibit a satellite mode at 1660 cm^{-1} and a combination band at 1750
223 cm^{-1} ($\nu_1 + \nu_4$). The MIR spectrum of the studied $\text{Ca}_{0.82}\text{Sr}_{0.18}\text{CO}_3$ solid solution differs from that of
224 calcite, as both of the ν_2 and ν_4 bending modes split into doublets separated by $\sim 10 \text{ cm}^{-1}$, and
225 additional modes appear at 1085 cm^{-1} (ν_1), 859 cm^{-1} , and at 1740 cm^{-1} (Fig. 4; S4). The
226 appearance of these new modes, in particular the IR-forbidden ν_1 band and the apparent splitting

of the bending modes, indicate clearly a lower crystalline symmetry of the solid solution compared to pure calcite, at least on the local scale (White, 1974). Similar IR features were previously observed in the infrared spectra of $\text{CaCO}_3\text{-II}$, collected in situ at 1.9 GPa (Koch-Müller et al., 2016), and in barytocalcite $\text{CaBa}(\text{CO}_3)_2$ ($P2_1/m$) (Scheetz and White, 1977). Both of these phases have structures derivative of calcite.

Raman spectra of $\text{Ca}_{0.82}\text{Sr}_{0.18}\text{CO}_3$ were collected at atmospheric pressure in the range of 100 – 1250 cm^{-1} (Fig. 5; S5; S6). The following modes are assigned to internal vibrations of the $(\text{CO}_3)^{2-}$ group: 1087 cm^{-1} with a satellite mode at 1066 cm^{-1} (ν_1), 711 cm^{-1} with a shoulder band at 706 cm^{-1} (ν_4), and a third peak at 875 cm^{-1} (ν_2) (Fig S6; S7). Three main low frequency bands located at 148, 190, and 275 cm^{-1} correspond to lattice vibrations (Fig S6). All bands, with the exception of the 706 cm^{-1} , 190 cm^{-1} , and 875 cm^{-1} can be assigned to calcite, yet shifted to lower wavenumbers due to the expansion of the unit cell caused by the presence of the larger Sr^{2+} cations (Fig. S5). The low intensity mode at 875 cm^{-1} (Fig. S6) corresponds to the out-of-plane bending vibration (ν_2), a Raman-inactive vibration in the calcite structure (White, 1974). As in the MIR case, the observation of additional modes indicates a lower symmetry of $\text{Ca}_{0.82}\text{Sr}_{0.18}\text{CO}_3$ compared to that of rhombohedral calcite.

Appearance of the additional lattice vibration mode at 190 cm^{-1} and the clear splitting of the ν_4 band on the Raman spectra was previously proposed as a main feature of the $\text{CaCO}_3\text{-II}$ polymorph (Pippinger et al., 2014). It should be noted, however, that while 190 cm^{-1} could be unequivocally distinguished in the spectra of $\text{Ca}_{0.82}\text{Sr}_{0.18}\text{CO}_3$, the splitting of ν_4 band is not apparent and the ‘extra’ component appears as a shoulder (Fig. S6). Possible reasons behind the absence of a clear ν_4 band splitting might be the spectral resolution, as well as the structural differences of $\text{Ca}_{0.82}\text{Sr}_{0.18}\text{CO}_3$ with $\text{CaCO}_3\text{-II}$ in a microstructural scale.

Overall, all of our collected data allow us to conclude that the structure of the synthesized $\text{Ca}_{0.82}\text{Sr}_{0.18}\text{CO}_3$ phase at ambient conditions has a lot of similarities with that of CaCO_3 -II, and can be viewed as a monoclinic distortion of the rhombohedral calcite structure. Therefore, we will call this new phase Sr-calcite-II.

High pressure Raman study

The results of the in situ high-pressure study of the $\text{Ca}_{0.82}\text{Sr}_{0.18}\text{CO}_3$ solid solution are summarized in Figs. 5 – 7 and in Supplementary materials Figs. S7 – S13. Since the Raman spectra of the detected high-pressure polymorphs are similar to those of CaCO_3 high-pressure modifications, the same nomenclature is used.

The Raman spectra collected in the compression experiments at room temperature are shown in Fig. 5 and 6. The first phase transition was detected at 1.8 GPa. New bands appear at 1080 cm^{-1} (Fig. 5; S7) and below 900 cm^{-1} , where we observe at least 10 new bands (Fig. 5; S9). The arising features of the Raman spectra are in good agreement with previous studies on the pure CaCO_3 system (Pippinger et al., 2014; Koch-Müller et al., 2016), resembling the CaCO_3 -IIIb Raman pattern. Thus, the $\text{Ca}_{0.82}\text{Sr}_{0.18}\text{CO}_3$ solid solution with CaCO_3 -IIIb-like structure will be called Sr-calcite-IIIb. Sr-calcite-IIIb was detected in the pressure range of 1.8 – 4 GPa (Fig. 1; S1).

Increase of pressure above 4 GPa leads to a clear and abrupt splitting of the 1100 cm^{-1} band in the Raman spectra (Fig. 5; S7; S8a). Previous studies in the CaCO_3 system attributed this splitting to the formation of CaCO_3 -III (Pippinger et al., 2014; Koch-Müller et al., 2016; Bayarjargal et al., 2018). Consequently, we conclude that Sr-calcite-III has appeared above 4 GPa. This phase was detected in a relatively narrow pressure range from 4 to 7 GPa (Fig. 1; S1).

Another clear change in the Raman spectra takes place above 7 GPa (Fig. 5; S7-S9). Even though, the spectra above 7 GPa contain similar set of modes as that of Sr-calcite-III, the bands above 1090 cm^{-1} broaden and shift abruptly to higher wavenumbers (Fig. 5; S7). The observed changes indicate the appearance of another structural modification. However, the Raman spectra cannot be explained by any known high-pressure polymorphs of CaCO_3 (Koch-Müller et al., 2016; Bayarjargal et al., 2018). Based on the similarities in the Raman spectra (Fig. 5; S7-S9), we assume that this new high-pressure modification has a closely related structure to that of Sr-calcite-III. Hence, we will refer to it as Sr-calcite-IIIc.

Sr-calcite-IIIc was detected as the only phase in the Raman spectra at room temperature from 7 to 14 GPa (Fig. 6). Further compression of Sr-calcite-IIIc leads to the formation of another high-pressure polymorph between 14 – 18 GPa (Fig. 6). The transition is sluggish and the sample transforms fully to the high-pressure phase at 20 GPa (Fig. 6). The Raman spectra collected at 20 GPa contain 13 intense bands in the range of 150 – 1250 cm^{-1} (Fig. 6; S10; S11). The external vibrational modes located below 500 cm^{-1} include at least 7 bands (Fig. 6; S11). The internal vibrational modes are represented by a single band at 1145 cm^{-1} (ν_1) with a shoulder on the high-frequency side, and two doublets at 733, 745 cm^{-1} (ν_4), and 862, 868 cm^{-1} (ν_2) (Fig. 6; S10; S11).

In pure CaCO_3 all previous studies showed formation of CaCO_3 -VI above 16 GPa at room temperature (Koch-Müller et al., 2016; Bayarjargal et al., 2018). However, the Raman spectra of the $\text{Ca}_{0.82}\text{Sr}_{0.18}\text{CO}_3$ solid solution show major differences from those of CaCO_3 -VI (Fig. S12). Raman spectra of CaCO_3 -VI contain a single ν_2 band (850 cm^{-1} at 20 GPa) (Bayarjargal et al., 2018), while the appearance of the two distinct bands at 850 – 890 cm^{-1} , as observed in the present study, was reported as the main feature of the CaCO_3 -VI to CaCO_3 -VII transition

(Bayarjargal et al., 2018) (Fig. S12). Based on our observations, we conclude that in the $\text{Ca}_{0.82}\text{Sr}_{0.18}\text{CO}_3$ solid solution, we observe the formation of a polymorph with a structure similar to CaCO_3 -VII (Sr-calcite-VII).

The Raman spectra of $\text{Ca}_{0.82}\text{Sr}_{0.18}\text{CO}_3$ solid solution measured between 20 – 55 GPa showed the persistence of Sr-calcite-VII up to the highest experimental pressure (Fig. 1; 6; S1). A new feature arising at 810 cm^{-1} at 44.6 GPa (Fig. 6; S10) may indicate the onset of a transition to a post-aragonite phase (Sr-post-aragonite further below) (Bayarjargal et al., 2018). Sr-calcite-VII and Sr-post-aragonite coexist between 44.6 – 55 GPa at room temperature (Fig. 6; S10). Formation of both phases at ambient temperature contrasts previous data on pure CaCO_3 , where the respective polymorphs were detected only after heating (Gavryushkin et al., 2017; Bayarjargal et al., 2018).

In the experimental runs 1 and 2 (Fig. S1), Raman spectra were measured also on decompression. The decompression of Sr-calcite-VII led to the formation of Sr-calcite-IIIc together with Sr-calcite-IIIb below 16 GPa (Fig. S1; S8b, c). Thus, Sr-calcite-IIIb could be observed in two pressure ranges from 1.8 to 4 GPa, and from 7 to 14 GPa (Fig. S1), same as reported by Koch-Müller et al (2016) for the CaCO_3 -IIIb. However, the ‘pressure stability window’ of Sr-calcite-IIIb depends on the experimental path.

For better understanding of the Sr-calcite-IIIc and Sr-calcite-IIIb behavior, additional high temperature Raman experiments were carried out at 9–10 GPa and 540 – 800 K (Fig. 1). First, pressure was increased to 9.4 GPa and Raman spectra were measured before heating (Fig. 7; S13). Sr-calcite-IIIc was detected at room temperature, confirming the previous observations. After less than 1 minute of heating, Sr-calcite-IIIc fully transformed to Sr-calcite-IIIb (Fig. 7; S13). Further heating led to the formation of an aragonite – type polymorph (Sr-aragonite)

already at 540 K and 9 GPa (Fig. 7; S13). Sr-aragonite is quenchable to atmospheric pressure, and was detected in the Raman spectra collected after experiments (Fig. S13).

Discussion

In this paper, we present the results of the first in situ experimental study on the CaCO_3 – SrCO_3 system, at pressures up to 55 GPa (Fig. 1; S1). The results of the present study show that incorporation of Sr^{2+} in CaCO_3 has a significant effect on the phase behavior of calcium carbonate at high pressures both at room and at high temperature. Below we discuss the findings of this work in detail, as well as their implications for understanding of the structural behavior of carbonates at mantle conditions.

The first synthesis experiment was performed at 2 GPa and 1273 K (1000 °C) (Fig. 1), which according to the CaCO_3 phase diagram, corresponds to the CaCO_3 -IV stability field, close to the calcite – aragonite transition curve (~2.5 GPa, 1273 K) (Ter Heege and Renner, 2007). The choice of the P – T synthesis parameters was influenced by the fact that a miscibility gap exists in the CaCO_3 – SrCO_3 system at low pressures (Chang and Brice 1972; Carlson, 1980). Due to the difference in the ionic radii of Ca^{2+} (1.00 Å) and Sr^{2+} (1.18 Å) (Shannon, 1976), miscibility of Sr^{2+} in the calcite structure is limited to 15 mol% at room temperature (Chang and Brice 1972; Carlson, 1980; Matsunuma et al., 2014) and approximately 40 mol% at 973 K (700 °C) (Chang and Brice 1972; Carlson, 1980). The coexisting phases in the miscibility gap have orthorhombic aragonite – type and rhombohedral calcite – type structures on the Sr-rich and Ca-rich sides, respectively (Chang and Brice 1972; Carlson, 1980). The two-phase field exists up to the transition to the CaCO_3 -IV anion-disordered phase ($R\bar{3}m$, disordered calcite structure) at 973 – 1173 K (700 – 900 °C) (Chang and Brice 1972; Carlson, 1980).

In this study we were able to synthesize a $\text{Ca}_{0.82}\text{Sr}_{0.18}\text{CO}_3$ solid solution at 2 GPa and 1273 K (1000 °C). The results of TEM (Fig. 2; S3) and EDS (Fig. S2) studies show textural and compositional homogeneity of the solid solution. The minor Sr-rich secondary phase was detected as small inclusions along the dislocations and cracks, which allows us to conclude that it is likely a relic of the growth media.

According to the XRD results, $\text{Ca}_{0.82}\text{Sr}_{0.18}\text{CO}_3$ is monoclinic at 2 GPa (Sr-calcite-II, space group $P2_1/c$). MIR- and Raman spectroscopy results show that Sr-calcite-II has a structure similar to that of CaCO_3 -II, which has been described as a monoclinic distortion of the calcite structure. CaCO_3 -II is a metastable phase which crystallizes in a narrow pressure range between 1.7 and 2.5 GPa (Pippinger et al., 2014). The majority of the experimental studies show that it is not quenchable to atmospheric pressure, and transforms to aragonite with heating (Merrill and Bassett, 1975; Pippinger et al., 2014; Koch-Müller et al., 2016; Bayarjargal et al., 2018). However, based on our observations, we can conclude that incorporation of Sr^{2+} in the solid solution expands the stability field of the CaCO_3 -II – like structure (Sr-calcite-II) to higher temperatures and lower pressures. Moreover, Sr-calcite-II is quenchable to ambient conditions.

As for the effect of cold compression, Sr-calcite-II was observed at room temperature up to 1.8 GPa. Further increase of pressure led to the formation of the following phases: i) Sr-calcite-IIIb at 1.8 – 4 GPa; ii) Sr-calcite-III at 4 – 7 GPa; iii) Sr-calcite-IIIC and/or IIIb at 7 – 16 GPa; iv) Sr-calcite-VII 16 – 55 GPa; vi) Sr-post-aragonite above 45 GPa (Fig. 1, S1).

The Raman spectra of the Sr-calcite-IIIb, III, and IIIC share a lot of similarities (Fig. S8; S9), and differ mostly in the symmetric stretching vibration regions ($900\text{--}1200\text{ cm}^{-1}$), composed of a single band with a shoulder for the Sr-calcite-IIIb modification, and doublets for the Sr-calcite-III and IIIC (Fig. S8, S9). Comparison of our spectroscopic results with previous

publications (Koch-Müller et al., 2016; Bayarjargal et al., 2018) shows that all phases have structures closely related to CaCO₃-III and IIIb. Moreover, the formation of Sr-calcite-IIIb and III phases in the solid solution occurs at the same $P - T$ conditions where the respective CaCO₃ polymorphs, CaCO₃-IIIb and III also appear (Fig. 1, S1) (Pippinger et al., 2014; Koch-Müller et al., 2016; Bayarjargal et al., 2018). The third phase, Sr-calcite-IIIc, is a unique modification, not observed in CaCO₃.

CaCO₃-IIIb and III structures are topologically similar and contain non co-planar CO₃²⁻ groups and two non-equivalent Ca coordination polyhedra (Ca^[7] and Ca^[9]) (Merlini et al., 2012). The main difference between them is in the arrangement of the structural blocks, which results in 10 (CaCO₃-III) and 4 (CaCO₃-IIIb) formula units, respectively, in the primitive unit cell (Merlini et al., 2012). According to DFT calculations, the increased number of atoms in the unit cell of CaCO₃-III as compared to CaCO₃-IIIb results in the splitting of the ν_1 , ν_2 , and ν_4 bands in the CaCO₃-III spectra (Koch-Müller et al., 2016). Taking into account the previous results on CaCO₃-III and IIIb, and the similarities of the Raman spectra of Sr-calcite-IIIb, III, and IIIc, we could speculate that those high pressure modifications have as well topologically similar structures (Koch-Müller et al., 2016; Bayarjargal et al., 2018). However, as the Raman spectroscopy does not give definite structural solutions, further single crystal XRD studies are necessary.

The similarity of Sr-calcite-IIIb and IIIc structures could explain the observed behavior of those phases at high pressure and temperature. Formation of Sr-calcite-IIIc or/and reappearance of Sr-calcite-IIIb occurs between 7 and 16 GPa and depends on the experimental $P - T$ path (Fig. 1; S1). Sr-calcite-IIIc forms in the cold compression experiments, while heating transforms it to

Sr-calcite-IIIb. In the decompression experiments at room temperature, Sr-calcite-IIIc and IIIb coexist in the 7-16 GPa pressure range (Fig. S1).

The observed dependence of the phase behavior on experimental $P - T$ path may result from the sensitivity of the Sr-calcite-IIIb and IIIc formation to the influence of the hydrostatic conditions. Both pressure media, Ar and NaCl, used in this study are non-hydrostatic at high pressure and room temperature (Klotz et al., 2009). Non-hydrostaticity may lead to the stress-induced phase transition at 7 GPa from Sr-calcite-III to Sr-calcite-IIIc. On the contrary, thermal annealing and/or pressure decrease can reduce the stress gradient (Angel et al., 2007) and promote formation of the Sr-calcite-IIIb polymorph at similar pressures. Sr-calcite-IIIb in the quasi-hydrostatic conditions forms in two pressure ranges between 1.8 – 4 GPa and at 7 – 16 GPa, showing similar behavior to CaCO_3 -IIIb (Koch-Müller et al., 2016).

The similar effect of the pressure medium, and the experimental $P - T$ path on the CaCO_3 -IIIb formation was previously observed in a number of experimental studies (i.e. Merlini et al., 2012, 2018; Yuan et al., 2018). In pure CaCO_3 , non-hydrostaticity suppresses the formation of CaCO_3 -IIIb and only CaCO_3 -III could be detected. The addition of Sr^{2+} to the system makes the effect more pronounced and leads to the new structural modification Sr-calcite-IIIc.

Sr-calcite-IIIb and IIIc are most likely metastable phases in the range of 7-16 GPa. They transform to the aragonite-structured polymorph, Sr-aragonite, already at 540 K and 9 GPa. The formation of Sr-aragonite is observed at approximately 200 K lower temperatures than in CaCO_3 (Fig 1).

Another high-pressure polymorph, Sr-calcite-VII appears already at room temperature and at 16 GPa, and it is stable until the highest pressure point investigated. Above 45 GPa Sr-calcite-VII probably coexists with the Sr-post-aragonite phase. The stability fields of both Sr-calcite-VII

and Sr-post-aragonite are located at approximately 10 – 15 GPa lower pressures than those of the respective CaCO_3 polymorphs (Ono, 2005; Gavryushkin et al., 2017; Bayarjargal et al., 2018). Both the formation of Sr-aragonite at much lower temperatures, as well as the appearance of Sr-calcite-VII and Sr-post-aragonite in the cold compression experiments, reveal a significant effect of Sr^{2+} on the kinetics of the pressure-induced structural transformations.

Even though the formation of the CaCO_3 polymorphs aragonite, CaCO_3 -VII, and post-aragonite is thermodynamically favored in the pure CaCO_3 system, it is kinetically hindered and occurs in experiments only above 773 K (500 °C) (Fig. 1) (Gavryushkin et al., 2017; Bayarjargal et al., 2018). On cold compression and at low temperatures, CaCO_3 transforms to metastable polymorphs, i.e. CaCO_3 -IIIb instead of aragonite at 7 – 15 GPa, and CaCO_3 -VI instead of CaCO_3 -VII and post-aragonite at 15 – 50 GPa (Koch-Müller et al., 2016; Bayarjargal et al., 2018).

The introduction of Sr^{2+} to CaCO_3 seems to lower the kinetic barrier that prevents the formation of aragonite, CaCO_3 -VII, and post-aragonite in the end member CaCO_3 , and promotes their formation at lower $P - T$ conditions. The observed tendency is most likely related to the capacity of the different Ca-carbonate high-pressure polymorphs to accommodate large cations. The known structures of aragonite, CaCO_3 -VII, and post-aragonite have larger cationic coordination numbers – 9, 10 and 12, respectively – than CaCO_3 -IIIb ($\text{Ca}^{[7]}$ - $\text{Ca}^{[9]}$) and CaCO_3 -VI ($\text{Ca}^{[7+2]}$) (Merlini et al., 2012; Gavryushkin et al., 2017). Ca-carbonate solid solutions with Sr^{2+} favor likely structures with larger coordination sites at lower pressures compared to pure CaCO_3 .

This tendency is in good agreement with previous observations in both end members (Wang et al., 2015) and the $\text{CaCO}_3 - \text{SrCO}_3$ solid solution (Carlson, 1980). Strontianite, SrCO_3 , tends to form structures with larger coordination numbers at a given pressure, compared to

CaCO₃: aragonite with Sr^[9] at atmospheric pressure, and post-aragonite with Sr^[12] already at 20 GPa (Wang et al., 2015). The small amounts of Sr²⁺ in CaCO₃ aragonite extend the stability field of aragonite structure to slightly lower pressures than in the unary CaCO₃ system (Carlson, 1980). The previous high pressure studies demonstrated formation of aragonite structured Ca_{0.80}Sr_{0.20}CO₃ solid solution at 1.6 GPa and 923 K, which in pure CaCO₃ system would still belong to the stability field of calcite (Carlson, 1980).

Our experiments show a significant role of the cation in the high-pressure phase transitions of calcium carbonate. The relatively small amount of Sr²⁺ in the synthesized solid solution, 18 mol%, comparable with that found in some diamond inclusions (Logvinova et al., 2008, 2011, 2019a), leads to significant changes in the phase diagram of calcium carbonate: i) stabilization at high temperatures of the CaCO₃-II – type structure (Sr-calcite-II); ii) stress-induced phase transition to the new high pressure modification, Sr-calcite-IIc; iii) formation of a polymorph with aragonite type structure at lower temperatures compared with that in CaCO₃; iv) phase transition to Sr-calcite-VII and Sr-post-aragonite already at room temperature and at pressures 10 – 15 GPa lower than in CaCO₃ (Fig. 1; S1).

The formation of monoclinic Sr-calcite-II at high temperatures raises the important question on whether the metastable CaCO₃ polymorphs can become thermodynamically stable in the other calcium carbonate solid solutions as well. For instance, previous studies reported that addition of 5 mol% of Fe²⁺ or Mg²⁺ to CaCO₃ stabilizes the calcite structure at 6 GPa and 1273 – 1473 K (1000 – 1200 °C) in the *P* – *T* stability field of CaCO₃ aragonite (Shatskiy et al., 2014, 2018; Müller et al., 2017). It is, however, unknown what structures Mg- or Fe-calcites adopt at high pressures and temperatures, as all previous studies examined the samples ex situ (Shatskiy et al., 2014, 2018; Müller et al., 2017).

One of the possibilities, proposed by Merlini et al. (2012), is the stabilization of CaCO₃-III – like structures in solid solutions with smaller cations. Due to the different polyhedral site volumes (Ca^[7]-Ca^[9]), the structure of CaCO₃-III could host cations with different ionic radii without a major elastic strain from non-ideal solid solution. The results of the present study show the fundamental possibility of the stabilization of metastable CaCO₃ phases in calcium carbonate solid solutions. Since CaCO₃-III transforms back to calcite with the release of pressure, it is necessary to study CaCO₃ – MgCO₃ and CaCO₃ – FeCO₃ in situ at high pressures.

Implications

The present study and previous observations (Shatskiy et al., 2014, 2018; Müller et al., 2017) show that the high pressure phase behavior of the calcium carbonate - based solid solutions depends strongly on the specific chemical composition of the solid solution. Even substituting a small amount of Ca²⁺ by different cation, such as smaller cations – Mg²⁺ or Fe²⁺, or bigger once – Sr²⁺ or Ba²⁺, shifts phase transition pressures and temperatures, and probably also leads to the formation of new crystal structures.

Due to the large coordination sites in aragonite, which is long believed to be the major calcium carbonate polymorph in the upper mantle, the solubility of Mg²⁺ and Fe²⁺ in the structure is limited to few mol% (Shatskiy et al., 2014, 2018; Müller et al., 2017), and higher concentrations will promote crystallization of phases with smaller cationic sites – either calcite, CaCO₃-III, or others, it is currently unknown. Indeed, natural aragonites contain only few mol% of Mg²⁺, Fe²⁺, while there are findings of Mg – rich and Fe – rich calcium carbonates with calcite structure in polycrystalline carbonate inclusions in garnets from diamond grade metamorphic rocks (Korsakov et al., 2010; Frezzotti et al., 2011). Thus, we could assume, that Mg²⁺ and Fe²⁺

impurities in calcium carbonates will prevent the aragonite formation at the upper mantle conditions down to at least 200 km depth (6 GPa).

On the contrary, the present experimental data show that structures with large cation sites – aragonite, CaCO_3 -VII, and post-aragonite are favorable and will likely be observed only in the pure CaCO_3 , in carbonates with larger cations, such as SrCO_3 and BaCO_3 , and in their solid solutions. Our high temperature experiments show that syngenetic (Sr,Ca)-carbonate inclusions in diamonds should have aragonite – type structure.

Because of the generally very small size of inclusions (Klein-BenDavid, 2006, 2009), that, furthermore, contain multi-phase assemblages of solid phases (silicates, oxides, carbonates), brines (halides), and fluid bubbles, the analytical techniques for the accurate investigation of the structures and compositions of the minerals are largely confined to TEM (Klein-BenDavid, 2006, 2009; Logvinova et al., 2008, 2011, 2019a; Kaminsky et al., 2009), IR and Raman spectroscopy (Logvinova et al., 2008, 2011, 2019a; Kaminsky et al., 2009). Most of the currently available studies on $(\text{Ba}, \text{Ca})\text{CO}_3$, $(\text{Sr}, \text{Ca})\text{CO}_3$ and $(\text{Ca}, \text{Ba}, \text{Sr})\text{CO}_3$ used the TEM method and IR spectroscopy and focused on the composition of the minerals rather than the structures (Klein-BenDavid, 2006, 2009; Logvinova et al., 2008, 2011, 2019a). However, in the paper by Kaminsky et al. (2009), Sr- and Ba-bearing calcium carbonate ($\text{Ca} = 99.26 \text{ mol.}\%$), that was found in the diamond nano-inclusions with the low mantle minerals walstromite-structured CaSiO_3 , CaTiO_3 and ferropericlase, was identified as rhombohedral calcite with the aid of Raman spectroscopy. According to the CaCO_3 phase diagram (Bayarjargal et al., 2018), at the low mantle conditions three carbonate phases could be stable: aragonite, CaCO_3 -VII and post-aragonite. Aragonite is quenchable to ambient conditions, while post-aragonite and CaCO_3 -VII transform back to calcite on decompression. Given that the addition of Sr^{2+} and Ba^{2+} stabilizes

both CaCO_3 -VII and post-aragonite type structures at lower pressures, we could assume that the crystallization of the $(\text{Ca}, \text{Ba}, \text{Sr})\text{CO}_3$ in the inclusions should have happened above 20-25 GPa likely in CaCO_3 -VII or post-aragonite type structures.

Inclusions in natural diamonds provide direct samples of the diamond forming media and could be used to reconstruct the physical-chemical environments in which their host diamonds were formed. $(\text{Ba}, \text{Ca})\text{CO}_3$, $(\text{Sr}, \text{Ca})\text{CO}_3$ and $(\text{Ca}, \text{Ba}, \text{Sr})\text{CO}_3$, despite the scarcity of the findings in inclusions of typical kimberlite and placer diamonds, are vivid indicators of metasomatic processes (Logvinova et al., 2008, 2011, 2019a). They appear in unique polyphase assemblages together with phosphates, halides, sheet silicates and abundant fluid segregations, and indicate the involvement of a carbonatitic high-density fluid/melt enriched in incompatible elements in the diamond formation (Cl, K, P, Ba and Sr) (Klein-BenDavid, 2006, 2009; Logvinova et al., 2008, 2011, 2019a). The carbon isotopic composition of the host diamonds, and predominant eclogitic paragenesis of mineral inclusions imply that this fluid/melt might have been supplied from the subducted rocks of the oceanic and continental lithosphere (Ragozin et al., 2009).

Thus, the data obtained experimentally in the studies of the carbonate phase diagrams, P - T parameters of the phase transitions, melting temperatures etc., are a useful tool for better understanding of the mantle processes and the reconstruction of their physical-chemical conditions. In particular, CaCO_3 - SrCO_3 and CaCO_3 - BaCO_3 systems are important for the reconstructions of the processes related to the carbonatites metasomatic activity.

The present study shows that the high pressure phase behavior of the calcium carbonate - based solid solutions depends strongly on the specific chemical composition of the solid solution. The structural changes derived from the cationic substitution can have an important impact on the phase diagrams of carbonates and, thus affect the physical properties of these materials such as

525 equations of state, sound velocities, melting temperatures etc, and should be considered in the
526 modeling of the processes, that involve carbonates. Overall, it is clear that the carbonate phase
527 diagrams in the complex multicomponent systems should be further studied with the use of in situ
528 methods.
529

References

- Angel, R.J., Bujak, M., Zhao, J., Gatta, G.D., and Jacobsen, S.D. (2007) Effective hydrostatic limits of pressure media for high-pressure crystallographic studies. *Journal of Applied Crystallography*, 40, 26-32.
- Bayarjargal, L., Fruhner, C.J., Schrodt, N., and Winkler, B. (2018) CaCO₃ phase diagram studied with Raman spectroscopy at pressures up to 50 GPa and high temperatures and DFT modeling. *Physics of the Earth and Planetary Interiors*, 281, 31-45.
- Brenker, F.E., Vollmer, C., Vincze, L., Vekemans, B., Szymanski, A., Janssens, K., Szaloki, I., Nasdala, L., Joswig, W., and Kaminsky, F. (2007) Carbonates from the lower part of transition zone or even the lower mantle. *Earth and Planetary Science Letters*, 260, 1-9.
- Carlson, W.D. (1980) The calcite–aragonite equilibrium: effects of Sr substitution and anion orientational disorder. *American Mineralogist*, 65, 1252-1262.
- Chang, L.L., and Brice, W.R. (1972) Subsolvus phase relations in aragonite-type carbonates: II. The systems CaCO₃-SrCO₃-PbCO₃ and CaCO₃-BaCO₃-PbCO₃. *American Mineralogist: Journal of Earth and Planetary Materials*, 57, 155-168.
- Dasgupta, R., and Hirschmann, M.M. (2006) Melting in the Earth's deep upper mantle caused by carbon dioxide. *Nature*, 440, 659-662.
- Datchi, F., Dewaele, A., Loubeyre, P., Letoullec, R., Le Godec, Y., and Canny, B. (2007) Optical pressure sensors for high-pressure–high-temperature studies in a diamond anvil cell. *High Pressure Research*, 27, 447-463.
- Dewaele, A., Torrent, M., Loubeyre, P., and Mezouar, M. (2008) Compression curves of transition metals in the Mbar range: Experiments and projector augmented-wave calculations. *Physical Review B*, 78, 104102.

- Frezzotti, M.L., Selverstone, J., Sharp, Z.D., and Compagnoni, R. (2011) Carbonate dissolution during subduction revealed by diamond-bearing rocks from the Alps. *Nature Geoscience*, 4, 703-706.
- Gavryushkin, P.N., Martirosyan, N.S., Inerbaev, T.M., Popov, Z.I., Rashchenko, S.V., Likhacheva, A.Y., Lobanov, S.S., Goncharov, A.F., Prakapenka, V.B., and Litasov, K.D. (2017) Aragonite-II and CaCO₃-VII: New High-Pressure, High-Temperature Polymorphs of CaCO₃. *Crystal Growth and Design*, 17, 6291-6296.
- Irving, A.J., and Wyllie, P.J. (1973) Melting relationships in CaO-CO₂ and MgO-CO₂ to 36 kilobars with comments on CO₂ in the mantle. *Earth and Planetary Science Letters*, 20, 220-225.
- Kamenetsky, V.S., and Yaxley, G.M. (2015) Carbonate-silicate liquid immiscibility in the mantle propels kimberlite magma ascent. *Geochimica et Cosmochimica Acta*, 158, 48-56.
- Kaminsky, F., Wirth, R., Matsyuk, S., Schreiber, A., and Thomas, R. (2009) Nyerereite and nahcolite inclusions in diamond: evidence for lower-mantle carbonatitic magmas. *Mineralogical Magazine*, 73, 797-816.
- Kaminsky, F.V., Wirth, R., and Schreiber, A. (2013) Carbonatitic inclusions in deep mantle diamonds from Juina, Brazil: new minerals in the carbonate-halide association. *The Canadian Mineralogist*, 51, 669-688.
- Kiseeva, E.S., Yaxley, G.M., Hermann, J., Litasov, K.D., Rosenthal, A. and Kamenetsky, V.S. (2012). An Experimental Study of Carbonated Eclogite at 3.5-5.5 GPa-Implications for Silicate and Carbonate Metasomatism in the Cratonic Mantle. *Journal of Petrology*, 53, 727-759.

- 575 Kiseeva, E.S., Litasov, K.D., Yaxley, G.M., Ohtani, E. and Kamenetsky, V.S. (2013). Melting
576 and phase relations of carbonated eclogite at 9–21 GPa and the petrogenesis of alkali-rich
577 melts in the deep mantle. *Journal of Petrology*, 54, 1555-1583.
- 578 Klein-BenDavid, O., Wirth, R. and Navon, O. (2006). TEM imaging and analysis of
579 microinclusions in diamonds: A close look at diamond-growing fluids. *American*
580 *Mineralogist*, 91, 353-365.
- 581 Klein-BenDavid, O., Logvinova, A.M., Schrauder, M., Spetius, Z.V., Weiss, Y., Hauri, E.H.,
582 Kaminsky, F.V., Sobolev, N.V. and Navon, O., (2009). High-Mg carbonatitic
583 microinclusions in some Yakutian diamonds – a new type of diamond-forming fluid.
584 *Lithos*, 112, 648-659.
- 585 Klotz, S., Chervin, J.C., Munsch, P., and Le Marchand, G. (2009) Hydrostatic limits of 11
586 pressure transmitting media. *Journal of Physics D: Applied Physics*, 42, 075413
- 587 Koch-Müller, M., Jahn, S., Birkholz, N., Ritter, E., and Schade, U. (2016) Phase transitions in the
588 system CaCO_3 at high P and T determined by in situ vibrational spectroscopy in diamond
589 anvil cells and first-principles simulations. *Physics and Chemistry of Minerals*, 43, 545-
590 561.
- 591 Korsakov, A.V., De Gussem, K., Zhukov, V.P., Perraki, M., Vandenabeele, P., and Golovin,
592 A.V. (2009) Aragonite-calcite-dolomite relationships in UHPM polycrystalline carbonate
593 inclusions from the Kokchetav Massif, northern Kazakhstan. *European Journal of*
594 *Mineralogy*, 21, 1301-1311.
- 595 Korsakov, A.V., De Gussem, K., Zhukov, V.P., Perraki, M., Vandenabeele, P., and Golovin,
596 A.V. (2010) Aragonite-calcite-dolomite relationships in UHPM polycrystalline carbonate

inclusions from the Kokchetav Massif, northern Kazakhstan. *European Journal of Mineralogy*, 21, 1301-1311.

Kuznetsov, A., Semikhatov, M., and Gorokhov, I. (2014) The Sr isotope chemostratigraphy as a tool for solving stratigraphic problems of the Upper Proterozoic (Riphean and Vendian). *Stratigraphy and Geological Correlation*, 22, 553-575.

Lobanov, S.S., Dong, X., Martirosyan, N.S., Samtsevich, A.I., Stevanovic, V., Gavryushkin, P.N., Litasov, K.D., Greenberg, E., Prakapenka, V.B., Oganov, A.R., and Goncharov, A.F. (2017) Raman spectroscopy and x-ray diffraction of sp^3 -CaCO₃ at lower mantle pressures. *Physical Review B*, 96, 104101

Logvinova, A.M., Wirth, R., Fedorova, E.N., and Sobolev, N.V. (2008) Nanometre-sized mineral and fluid inclusions in cloudy Siberian diamonds: new insights on diamond formation. *European Journal of Mineralogy*, 20, 317-331.

Logvinova, A.M., Wirth, R., Tomilenko, A.A., Afanas'ev, V.P., and Sobolev, N.V. (2011) The phase composition of crystal-fluid nanoinclusions in alluvial diamonds in the northeastern Siberian Platform. *Russian Geology and Geophysics*, 52, 1286-1297.

Logvinova, A., Zedgenizov, D., and Wirth, R. (2019a) Specific Multiphase Assemblages of Carbonatitic and Al-Rich Silicic Diamond-Forming Fluids/Melts: TEM Observation of Microinclusions in Cuboid Diamonds from the Placers of Northeastern Siberian Craton. *Minerals*, 9 (1), 50

Logvinova, A.M., Shatskiy, A., Wirth, R., Tomilenko, A.A., Ugap'eva, S.S., and Sobolev, N.V. (2019b) Carbonatite melt in type Ia gem diamond. *Lithos*, 342, 463-467.

- 618 Matsunuma, S., Kagi, H., Komatsu, K., Maruyama, K., and Yoshino, T. (2014) Doping
619 incompatible elements into calcite through amorphous calcium carbonate. *Crystal Growth*
620 *& Design*, 14, 5344-5348.
- 621 Merlini, M., Hanfland, M., and Crichton, W.A. (2012) CaCO₃-III and CaCO₃-VI, high-pressure
622 polymorphs of calcite: Possible host structures for carbon in the Earth's mantle. *Earth and*
623 *Planetary Science Letters*, 333, 265-271.
- 624 Merlini, M., Crichton, W.A., Chantel, J., Guignard, J., and Poli, S. (2018) Evidence of
625 interspersed co-existing CaCO₃-III and CaCO₃-IIIb structures in polycrystalline CaCO₃ at
626 high pressure. *Mineralogical Magazine*, 78, 225-233.
- 627 Merrill, L., and Bassett, W.A. (1975) The crystal structure of CaCO₃ (II), a high-pressure
628 metastable phase of calcium carbonate. *Acta Crystallographica Section B: Structural*
629 *Crystallography and Crystal Chemistry*, 31, 343-349.
- 630 Müller, J., Koch-Müller, M., Rhede, D., Wilke, F.D., and Wirth, R. (2017) Melting relations in
631 the system CaCO₃-MgCO₃ at 6 GPa. *American Mineralogist*, 102, 2440-2449.
- 632 Ono, S., Kikegawa, T., Ohishi, Y., and Tsuchiya, J., (2005) Post-aragonite phase transformation
633 in CaCO₃ at 40 GPa. *American Mineralogist*, 90, 667-671.
- 634 Ono, S., Kikegawa, T., and Ohishi, Y. (2007) High-pressure transition of CaCO₃. *American*
635 *Mineralogist*, 92, 1246-1249.
- 636 Palyanov, Y.N., Sokol, A., Borzdov, Y.M., Khokhryakov, A., and Sobolev, N. (1999) Diamond
637 formation from mantle carbonate fluids. *Nature*, 400, 417-418.
- 638 Pippinger, T., Miletich, R., Merlini, M., Lotti, P., Schouwink, P., Yagi, T., Crichton, W.A., and
639 Hanfland, M. (2014) Puzzling calcite-III dimorphism: crystallography, high-pressure

behavior, and pathway of single-crystal transitions. *Physics and Chemistry of Minerals*,
42, 29-43.

Ragozin, A., Shatskii, V. and Zedgenizov, D. (2009). New data on the growth environment of
diamonds of the variety V from placers of the northeastern Siberian platform. *Doklady
Earth Sciences*, 425 (2), 436.

Romanenko, A.V., Rashchenko, S.V., Kurnosov, A., Dubrovinsky, L., Goryainov, S.V.,
Likhacheva, A.Y. and Litasov, K.D. (2018) Single-standard method for simultaneous
pressure and temperature estimation using $\text{Sm}^{2+}:\text{SrB}_4\text{O}_7$ fluorescence. *Journal of Applied
Physics*, 124, 165902.

Scheetz, B., and White, W. (1977) Vibrational spectra of the alkaline earth double carbonates.
American Mineralogist, 62, 36-50.

Shannon, R.D. (1976). Revised effective ionic radii and systematic studies of interatomic
distances in halides and chalcogenides. *Acta crystallographica section A: crystal physics,
diffraction, theoretical and general crystallography*, 32, 751-767.

Sharygin, I.S., Litasov, K.D., Shatskiy, A., Golovin, A.V., Ohtani, E., and Pokhilenko, N.P.
(2015) Melting phase relations of the Udachnaya-East Group-I kimberlite at 3.0–6.5 GPa:
Experimental evidence for alkali-carbonatite composition of primary kimberlite melts and
implications for mantle plumes. *Gondwana Research*, 28, 1391-1414.

Shatskiy, A., Borzdov, Y.M., Litasov, K.D., Kupriyanov, I.N., Ohtani, E., and Palyanov, Y.N.
(2014) Phase relations in the system $\text{FeCO}_3\text{-CaCO}_3$ at 6 GPa and 900-1700 °C and its
relation to the system $\text{CaCO}_3\text{-FeCO}_3\text{-MgCO}_3$. *American Mineralogist*, 99, 773-785.

- 661 Shatskiy, A., Podborodnikov, I.V., Arefiev, A.V., Minin, D.A., Chanyshv, A.D., and Litasov,
662 K.D. (2018) Revision of the CaCO_3 – MgCO_3 phase diagram at 3 and 6 GPa. American
663 Mineralogist, 103, 441-452.
- 664 Stachel, T., and Harris, J. (2008) The origin of cratonic diamonds – constraints from mineral
665 inclusions. Ore Geology Reviews, 34, 5-32.
- 666 Stachel, T., Harris, J.W., Brey, G.P., and Joswig, W. (2000) Kankan diamonds (Guinea) II: lower
667 mantle inclusion parageneses. Contributions to Mineralogy and Petrology, 140, 16-27.
- 668 Suito, K., Namba, J., Horikawa, T., Taniguchi, Y., Sakurai, N., Kobayashi, M., Onodera, A.,
669 Shimomura, O., and Kikegawa, T. (2001) Phase relations of CaCO_3 at high pressure and
670 high temperature. American Mineralogist, 86, 997-1002.
- 671 Ter Heege, J.H., and Renner, J. (2007) In situ impedance spectroscopy on pyrophyllite and
672 CaCO_3 at high pressure and temperature: phase transformations and kinetics of atomistic
673 transport. Physics and Chemistry of Minerals, 34, 445-465.
- 674 Vahur, S., Teearu, A., Peets, P., Joosu, L., and Leito, I. (2016) ATR-FT-IR spectral collection of
675 conservation materials in the extended region of $4000\text{--}80\text{ cm}^{-1}$. Analytical and
676 Bioanalytical Chemistry, 408, 3373-3379.
- 677 Walker, D., Carpenter, M., and Hitch, C. (1990) Some simplifications to multianvil devices for
678 high pressure experiments. American Mineralogist, 75, 1020-1028.
- 679 Wang, M., Liu, Q., Nie, S., Li, B., Wu, Y., Gao, J., Wei, X., and Wu, X. (2015) High-pressure
680 phase transitions and compressibilities of aragonite-structure carbonates: SrCO_3 and
681 BaCO_3 . Physics and Chemistry of Minerals, 42, 517-527.
- 682 White, W.B. (1974) The carbonate minerals. In V.C. Farmer, Ed., The Infrared Spectra of the
683 Minerals, p. 227–284. Monograph, Mineralogical Society, London.

- 684 Yaxley, G.M., Crawford, A.J., and Green, D.H. (1991) Evidence for carbonatite metasomatism in
685 spinel peridotite xenoliths from western Victoria, Australia. Earth and Planetary Science
686 Letters, 107, 305-317.
- 687 Yuan, X., Gao, C., and Gao, J. (2018) An in situ study of the phase transitions among CaCO_3
688 high-pressure polymorphs. Mineralogical Magazine, 83, 191-197.
- 689

Figure captions

Fig. 1. Experimental conditions and phase identification of (Ca, Sr)CO₃ solid solution in comparison with CaCO₃ phase diagram. Symbols show the P-T conditions of the present study. For more details on the room temperature experiments see Inset and Fig. S1. Detected polymorphs are marked with different colors (also shown in the legend). Seven high P phases of (Ca, Sr)CO₃ were detected: Sr-calcite-II (Sr-CC-II); Sr-calcite-IIIb (Sr-CC-IIIb); Sr-calcite-III (Sr-CC-III); Sr-calcite-IIIc (Sr-CC- IIIc); Sr-calcite-VII (Sr-CC-VII); Sr-aragonite (Sr- Arag) and Sr-post-aragonite (Sr-Post-Arag). Black text and lines represent the known phase diagram of CaCO₃ (Irving and Wyllie, 1973; Suito, 2001; Ono, 2005; Ter Heege and Renner, 2007; Pippinger et al., 2014; Koch-Müller et al., 2016; Gavryushkin et al., 2017; Bayarjargal et al., 2018).

Fig. 2. Results of the TEM analysis performed on the Ca_{0.82}Sr_{0.18}CO₃ solid solution: (a) the lamellar texture of the sample, (b) the electron diffraction pattern. The lines in (b) represent the unit cell of calcite with *R*-3*c* space group with *a* = 5.01 Å and *c* = 17.25 Å. The EDX spectra are given in supplementary materials Fig. S3.

Fig. 3. The results of the Pawley refinement for the Ca_{0.82}Sr_{0.18}CO₃ solid solution (Sr-calcite-II) using (a, b) calcite (*R*-3*c*) and (c,d) CaCO₃-II (*P*2₁/*c*) as a model. The XRD patterns were obtained at ambient conditions. Insets on top (b, c) show magnified region with splitted peaks. The calculated Bragg reflection positions of CaCO₃-II and calcite are marked with red vertical bars; experimental patterns – dark blue crosses, calculated patterns – green line; difference profiles – blue line; and background profiles – red line.

Fig. 4. Mid IR spectrum of the Ca_{0.82}Sr_{0.18}CO₃, Sr-calcite-II (Sr-CC-II), in comparison with spectrum of CaCO₃ calcite (from IR database (Vahur et al., 2016)). The spectrum of calcite

contains 4 modes (shown by gray dashed lines): 712 cm^{-1} (ν_4); 872 cm^{-1} (ν_2); 1407 cm^{-1} (ν_3); and 1750 cm^{-1} ($\nu_1 + \nu_4$). In the MIR spectrum of the Sr-CC-II the ν_2 and ν_4 bending modes are splitted, additional modes appear at 1085 cm^{-1} (ν_1), 859 cm^{-1} , and at 1740 cm^{-1} (all marked by arrows). The fitting of the bands of the $\text{Ca}_{0.82}\text{Sr}_{0.18}\text{CO}_3$ spectrum is illustrated in Fig. S4

Fig. 5. Raman spectra of $\text{Ca}_{0.82}\text{Sr}_{0.18}\text{CO}_3$ solid solution collected upon compression up to 7 GPa. Four high – pressure phases were observed: Sr-calcite-II (Sr-CC-II), Sr-calcite-IIIb (Sr-CC- IIIb), Sr-calcite-III (Sr-CC- III) and Sr-calcite-IIIc (Sr-CC- IIIc). Raman spectrum collected before the experiment is shown in black. For more details see run 3 in Fig. S1

Fig. 6. Raman spectra collected at 14 – 50 GPa (see run 3 and 4 in Fig. S1) showing formation of Sr-calcite-VII (Sr-CC-VII) and Sr-post-aragonite (Post-Arag) in the room temperature experiments. The Sr-post-aragonite band appears around 44.6 GPa (marked by arrows).

Fig. 7. Transformation of Sr-calcite-IIIc (Sr-CC-IIIc) to Sr-calcite-IIIb (Sr-CC-IIIb) and Sr-aragonite (Arag) at high temperature and 9 – 10 GPa. P - T conditions and time from the beginning of heating (t) at which spectrum was collected are shown on the figures. The characteristic Sr-aragonite peak is marked by the arrows.

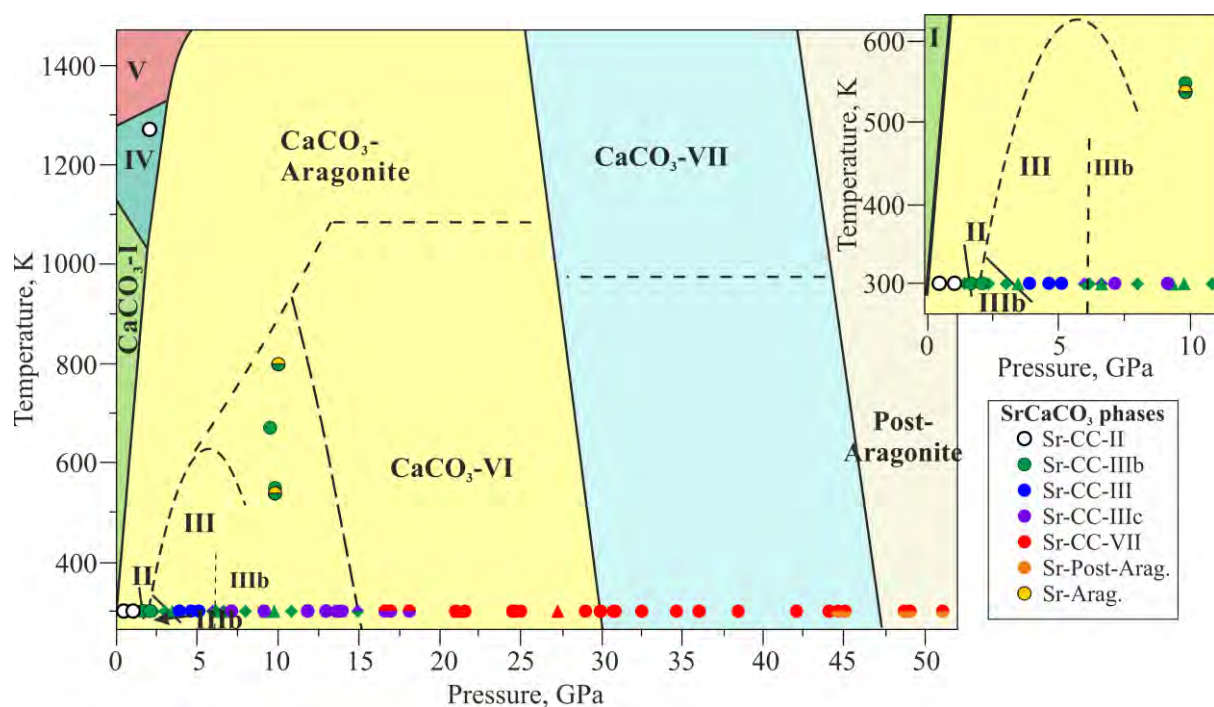


Fig. 1. Experimental conditions and phase identification of (Ca, Sr)CO₃ solid solution in comparison with CaCO₃ phase diagram. Symbols show the *P-T* conditions of the present study. For more details on the room temperature experiments see Inset and Fig. S1. Detected polymorphs are marked with different colors (also shown in the legend). Seven high *P* phases of (Ca, Sr)CO₃ were detected: Sr-calcite-II (Sr-CC-II); Sr-calcite-IIIb (Sr-CC-IIIb); Sr-calcite-III (Sr-CC-III); Sr-calcite-IIIc (Sr-CC- IIIc); Sr-calcite-VII (Sr-CC-VII); Sr-aragonite (Sr- Arag) and Sr-post-aragonite (Sr-Post-Arag). Black text and lines represent the known phase diagram of CaCO₃ (Irving and Wyllie, 1973; Suito, 2001; Ono, 2005; Ter Heege and Renner, 2007; Pippinger et al., 2014; Koch-Müller et al., 2016; Gavryushkin et al., 2017; Bayarjargal et al., 2018).

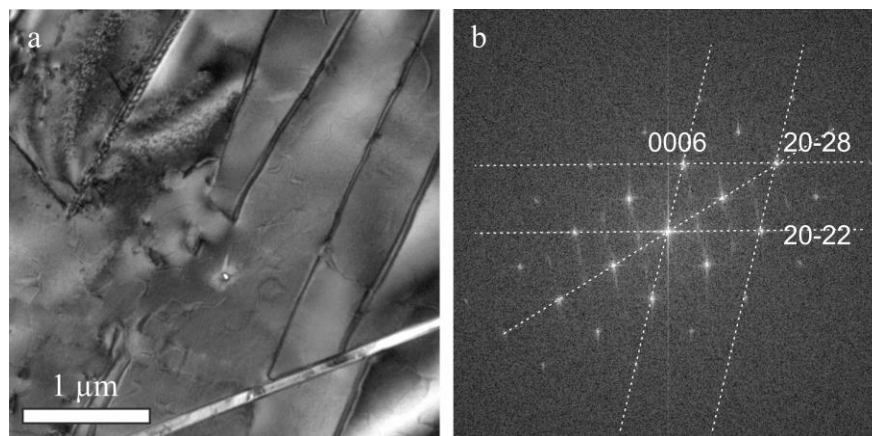


Fig. 2. Results of the TEM analysis performed on the $\text{Ca}_{0.82}\text{Sr}_{0.18}\text{CO}_3$ solid solution: **(a)** the lamellar texture of the sample, **(b)** the electron diffraction pattern. The lines in **(b)** represent the unit cell of calcite with *R*-3*c* space group with $a = 5.01 \text{ \AA}$ and $c = 17.25 \text{ \AA}$. The EDX spectra are given in supplementary materials Fig. S3.

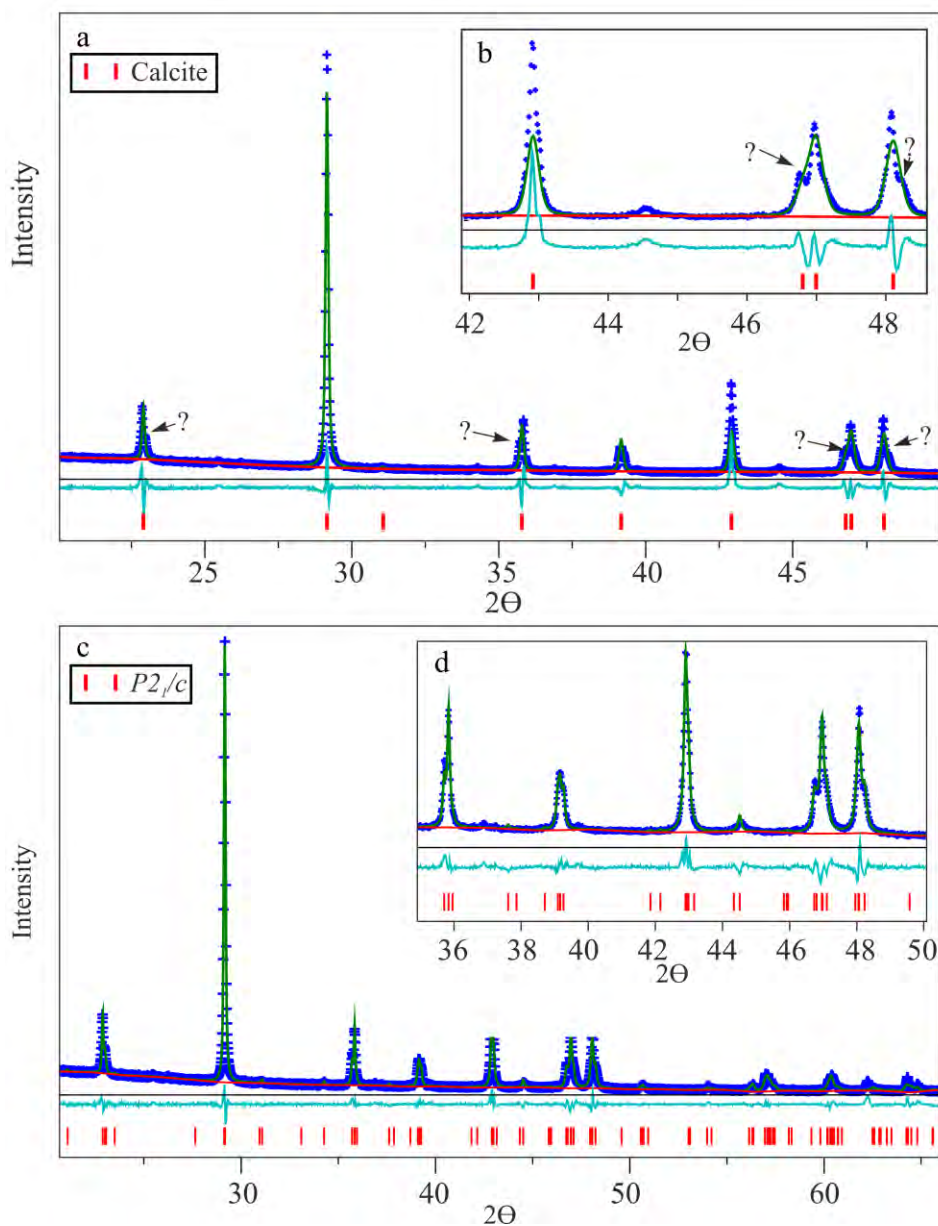


Fig. 3. The results of the Pawley refinement for the $\text{Ca}_{0.82}\text{Sr}_{0.18}\text{CO}_3$ solid solution (Sr-calcite-II) using (a, b) calcite ($R\text{-}3c$) and (c,d) $\text{CaCO}_3\text{-II}$ ($P2_1/c$) as a model. The XRD patterns were obtained at ambient conditions. Insets on top (b, c) show magnified region with splitted peaks. The calculated Bragg reflection positions of $\text{CaCO}_3\text{-II}$ and calcite are marked with red vertical bars; experimental patterns – dark blue crosses, calculated patterns – green line; difference profiles – blue line; and background profiles – red line.

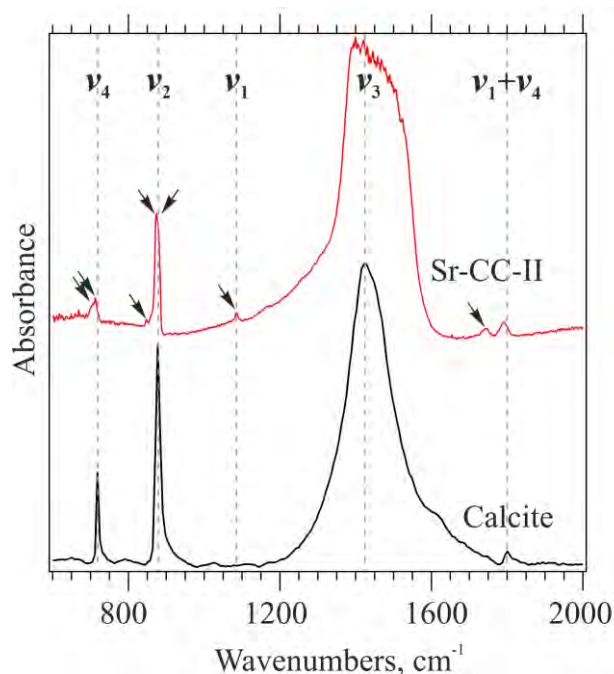


Fig. 4. Mid IR spectrum of the $\text{Ca}_{0.82}\text{Sr}_{0.18}\text{CO}_3$, Sr-calcite-II (Sr-CC-II), in comparison with spectrum of CaCO_3 calcite (from IR database (Vahur et al., 2016)). The spectrum of calcite contains 4 modes (shown by gray dashed lines): 712 cm^{-1} (ν_4); 872 cm^{-1} (ν_2); 1407 cm^{-1} (ν_3); and 1750 cm^{-1} ($\nu_1 + \nu_4$). In the MIR spectrum of the Sr-CC-II the ν_2 and ν_4 bending modes are splitted, additional modes appear at 1085 cm^{-1} (ν_1), 859 cm^{-1} , and at 1740 cm^{-1} (all marked by arrows). The fitting of the bands of the $\text{Ca}_{0.82}\text{Sr}_{0.18}\text{CO}_3$ spectrum is illustrated in Fig. S4

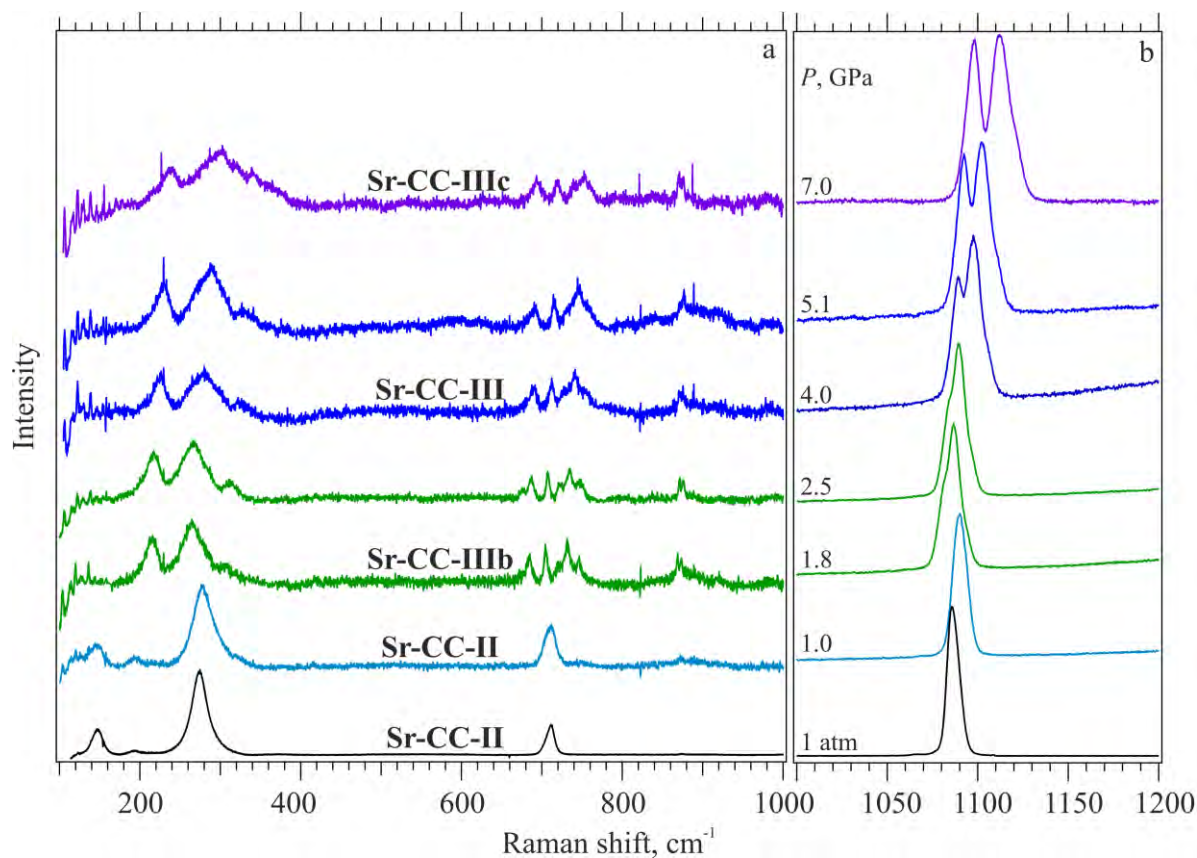


Fig. 5. Raman spectra of $\text{Ca}_{0.82}\text{Sr}_{0.18}\text{CO}_3$ solid solution collected upon compression up to 7 GPa. Four high – pressure phases were observed: Sr-calcite-II (Sr-CC-II), Sr-calcite-IIIb (Sr-CC- IIIb), Sr-calcite-III (Sr-CC- III) and Sr-calcite-IIIc (Sr-CC- IIIc). Raman spectrum collected before the experiment is shown in black. For more details see run 3 in Fig. S1

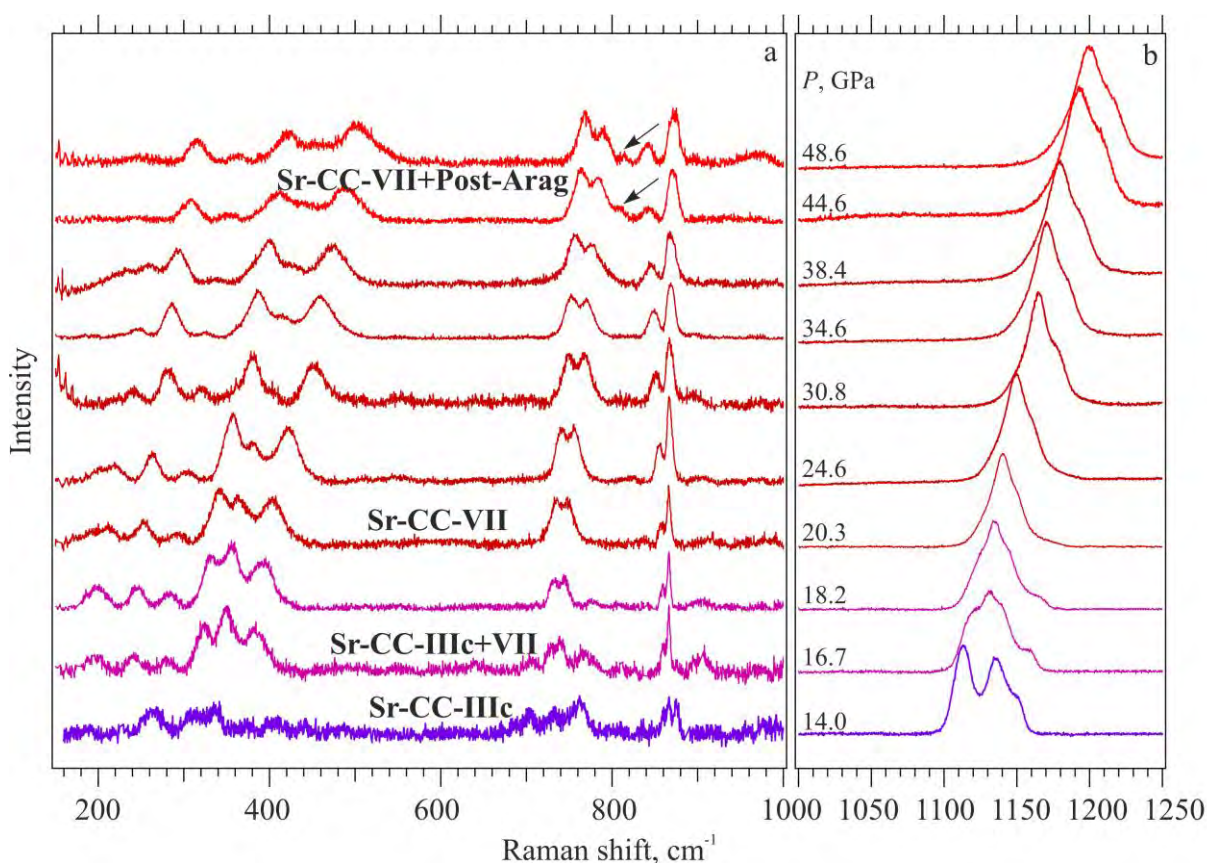


Fig. 6. Raman spectra collected at 14 – 50 GPa (see run 3 and 4 in Fig. S1) showing formation of Sr-calcite-VII (Sr-CC-VII) and Sr-post-aragonite (Post-Arag) in the room temperature experiments. The Sr-post-aragonite band appears around 44.6 GPa (marked by arrows).

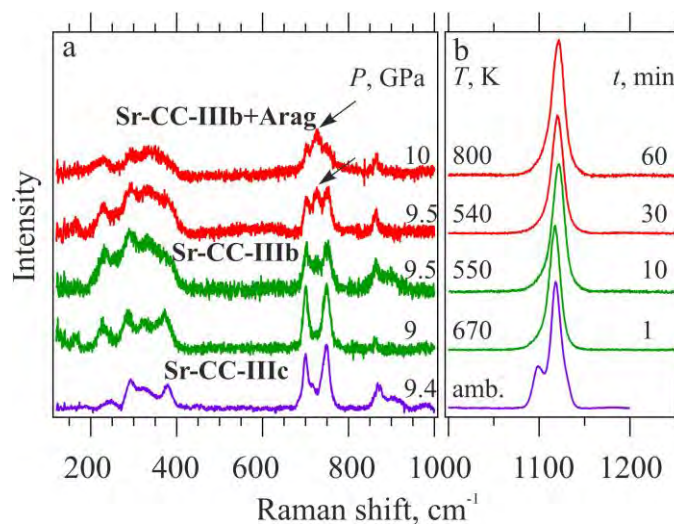


Fig. 7. Transformation of Sr-calcite-IIIc (Sr-CC-IIIc) to Sr-calcite-IIIb (Sr-CC-IIIb) and Sr-aragonite (Arag) at high temperature and 9 – 10 GPa. P - T conditions and time from the beginning of heating (t) at which spectrum was collected are shown on the figures. The characteristic Sr-aragonite peak is marked by the arrows.